

## **AlGaAs diodes for X-ray spectroscopy**

J.E. Lees<sup>\*1</sup>, D.J. Bassford<sup>1</sup>, J. S. Ng<sup>2</sup>, C. H. Tan<sup>2</sup>, and  
J. P. R. David<sup>2</sup>

### **Abstract**

$\text{Al}_{0.8}\text{Ga}_{0.2}\text{As}$   $\text{p}^+\text{-p}^-\text{-n}^+$  diodes with low reverse leakage currents ( $<10\text{nA}$ ) were evaluated as room temperature ( $23^\circ\text{C}$ ), soft X-ray photon counting detectors. X-ray spectra from a  $^{55}\text{Fe}$  radioactive source show these diodes can be used for spectroscopy with promising energy resolution of 1.47 keV FWHM at 5.9 keV. At elevated reverse bias levels ( $>20\text{V}$ ) we observed avalanche multiplication which, while improving the signal-to-noise ratio, degraded the spectroscopic performance.

*PACS:* 07.85.Fv, 29.40.Wk

*Keywords:* X-ray detection, AlGaAs, avalanche multiplication.

\*Corresponding author: +44 116 252 5519, E-mail address [lee@star.le.ac.uk](mailto:lee@star.le.ac.uk)

<sup>1</sup>Space Research Centre, Department of Physics and Astronomy, Michael Atiyah Building, University of Leicester, Leicester, LE1 7RH, UK.

<sup>2</sup> Department of Electronic & Electrical Engineering, University of Sheffield, Mappin Street, Sheffield, S1 3JD, UK.

## 1. Introduction

The material  $\text{Al}_x\text{Ga}_{1-x}\text{As}$  is widely used in GaAs-based electronic and optoelectronic devices. Any composition of  $\text{Al}_x\text{Ga}_{1-x}\text{As}$  can be grown lattice-matched to the GaAs substrates, which are commercially available in diameters of 150 mm. As a result, using current epitaxial wafer growth technologies high quality  $\text{Al}_x\text{Ga}_{1-x}\text{As}$  material of reasonable thickness (several microns) are achievable with negligible growth defects. With high quality material growth and large band gaps of high Al-content  $\text{Al}_x\text{Ga}_{1-x}\text{As}$ , e.g. 2.09 eV for  $\text{Al}_{0.8}\text{Ga}_{0.2}\text{As}$  [1],  $\text{Al}_x\text{Ga}_{1-x}\text{As}$  diodes tend to exhibit low intrinsic reverse leakage current at room temperature without any device passivation [2]. Large band gap  $\text{Al}_x\text{Ga}_{1-x}\text{As}$  may thus be suitable for X-ray detection at room temperature.

In optical signal detection, avalanche photodiodes (APDs), whose avalanche multiplication factor,  $M$ , increases with the device reverse bias, are often used in detection systems [3] to improve the system overall signal-to-noise ratio. Silicon-based APDs have been used for X-ray detection for many applications. Recent work by Kataoka et al [4] have also shown that good spectroscopic performance can also be maintained in addition to the avalanche multiplication.

However, there has been no report in the literature of using  $\text{Al}_x\text{Ga}_{1-x}\text{As}$  diodes for room temperature X-rays detection. This paper presents results of  $\text{Al}_x\text{Ga}_{1-x}\text{As}$  diodes used for soft X-ray photon counting detection and reports observation of avalanche multiplication effects in the X-ray spectra. Associated characterisation results (electrical and avalanche multiplication) are presented along with X-ray detection spectra.

## 2. Wafer structure and device fabrication

The wafer used in this study is an  $\text{Al}_{0.8}\text{Ga}_{0.2}\text{As}$   $\text{p}^+\text{-p}^-\text{-n}^+$  diode grown on an  $\text{n}^+$  (100) on-axis GaAs substrate (thickness of 350  $\mu\text{m}$ ) by a VG V80 Molecular Beam Epitaxy (MBE) machine. The substrate was supplied polished (epi-ready) by Wafer Technology [5] so no preparation other than the standard surface oxide removal (carried out in the MBE machine) was required.

The epitaxial layer material thickness and deduced doping density are given in Table 1. Although the wafer was originally intended to be an  $\text{Al}_{0.8}\text{Ga}_{0.2}\text{As}$   $\text{p}^+\text{-i-n}^+$  diode, doping information deduced from devices fabricated from the wafer indicate that that the structure resembles a  $\text{p}^+\text{-n}^-\text{-n}^+$  diode.

The doping density details in Table 1 were estimated from reverse bias Capacitance-Voltage (C-V) measurements performed on devices whose fabrication details will be described later. The C-V measurements were carried out at room temperature by directly probing the devices and using a Hewlett Packard 4275 LCR meter with the ac test voltage signal magnitude and frequency set at 50 mV rms and 1 MHz, respectively. The C-V data were fitted using an electrostatic model (Poisson's equation) assuming an abrupt 3-region  $p^+n^-n^+$  doping profile and a dielectric constant of 10.7 for the  $Al_{0.8}Ga_{0.2}As$  layers [6]. The doping density in the Si-doped  $Al_{0.8}Ga_{0.2}As$  layer (Layer 4) was assumed to be  $2 \times 10^{18} \text{ cm}^{-3}$ , and the unintentionally doped  $Al_{0.8}Ga_{0.2}As$  layer was assumed to be n-type. The adjustable parameters in the electrostatic model are doping densities of Layers 2 and 3 as well as the thickness of Layer 3.

Circular mesa devices were fabricated from the wafer using standard optical lithography and a Hydrobromic Acid: Acetic Acid: Potassium Dichromate (1:1:1) wet chemical etching. Each device had an Au/Zn/Au ohmic contact (annealed at 360 °C) to the top p-GaAs layer. In/Ge/Au alloy was deposited to the back  $n^+$  substrate and then annealed at 420 °C to provide the ohmic n-metal contact. Most of the devices had optical windows. Four sizes of diodes were fabricated having radii of 25, 50, 100, and 200  $\mu\text{m}$ . Only the two largest sizes of device (both with optical windows) were wire-bonded for subsequent X-ray detection measurements. There was no passivation on the mesa sidewalls. A photograph of the fabricated devices is shown in Fig. 1.

### 3. Experiments and results

#### 3.1 Avalanche multiplication

Avalanche multiplication factor versus reverse bias characteristics were measured on the devices using photomultiplication measurements [2]. In these measurements, carriers are generated by photon absorption outside the high-field region, before diffusing into the high-field region.

Laser light from a 442nm wavelength continuous-wave He-Cd laser was focused onto the optical window of the device under test. Electron-hole-pairs were generated in the p- $Al_{0.8}Ga_{0.2}As$  cladding due to photon absorption (97% of the light is absorbed in the  $\sim 1 \mu\text{m}$  thick p- $Al_{0.8}Ga_{0.2}As$  cladding). The electrons diffuse and are

collected by the depletion region. This procedure ensures pure electron injection into the high-field region and allows measurement of the multiplication factor due to pure electron injection,  $M_e$ .

The laser light was modulated by a mechanical chopper to enable phase-sensitive detection of the photocurrent, which distinguishes the photocurrent from device leakage current. The photocurrent was measured via voltage dropped across a series resistor using a lock-in amplifier, while the device was reverse-biased by a Keithley 236 Source-Measure-Unit. Multiplication factors were obtained by normalising the photocurrent data to the injected photocurrent. Slight increase in carrier collection efficiency with reverse bias, which affects the injected photocurrent, was accounted for in the analyses [7].

Measurements of the multiplication factor due to pure hole injection,  $M_h$ , were carried out on a batch of devices with the substrate removed through mechanical polishing and chemical etching. For these measurements, the 442nm wavelength laser light was focused onto the back of the device (GaAs substrate), injecting holes into the high field region. The same procedure as for measuring  $M_e$  was followed to obtain the hole multiplication factor,  $M_h$ . The photomultiplication data of  $M_e$  and  $M_h$  for the devices are plotted against reverse bias in Fig. 2. Any other mixed carrier injection condition will give rise to mixed multiplication factor,  $M_{mix}$ , that must be within the range of  $M_e$  and  $M_h$ .

### 3.2 Electrical characterisation

Reverse bias current-voltage characteristics of the diodes were measured using a calibrated Keithley 427 ammeter in order to assess suitability of the diodes for subsequent X-ray measurements (Section 3.3). The devices exhibited sufficiently low (<10 nA) leakage current up to reverse bias of 26 V. Smaller devices showed lower leakage current than larger devices for a given reverse bias, as expected from device area and/or perimeter scaling of leakage currents.

Devices D1 and D2, with radii of 100 and 200  $\mu\text{m}$ , respectively, were chosen for X-ray measurements. From the C-V measurements described earlier, for reverse bias greater than 10 V, the capacitance values are  $\sim 5$  and  $\sim 20$  pF, for D1 and D2, respectively, scaling with device area as expected.

### 3.3 X-Ray spectra

For X-ray measurement, a  $^{55}\text{Fe}$  radioactive source (0.15 MBq) which gives characteristic Mn  $K_\alpha$  and  $K_\beta$  peaks (5.9 keV and 6.4 keV respectively), was used as the X-ray source and was placed at a constant distance of approximately 3 cm above the diode under test. The diode was connected to a charge sensitive preamplifier, which had a JFET (Vishay Siliconix 2N4416, capacitance  $\sim 2$  pF) as the input transistor. Output signal from the preamplifier was then modified by a shaping amplifier (Ortec 571), which was in turn connected to a multi-channel analyser (MCA) to collect the spectrum. The event threshold was adjusted by varying the input discriminator level of the MCA such that number of noise events was minimised. All measurements were carried out at room temperature (23°C) without cooling of the diode under test. Data accumulation time for each spectrum was 24 hours.

Fig. 3 shows the spectra obtained from D2 as a function of reverse bias voltage. Similar spectra were obtained from D1 (not shown here), but with lower efficiency due to the smaller X-ray sensitive area in D1 compared to D2. As reverse bias increases, the main X-ray peak channel number increases, moving away from the noise peak, improving the overall signal to noise ratio.

Next, we compare the dependence of the main peak channel number (Fig. 3) as a function of reverse bias with the experimental avalanche multiplication characteristics shown in Fig. 2. The peak channel number from Fig. 3 was normalised to the value measured for a reverse bias of 15 V then scaled to value of the mixed carrier injection multiplication,  $M_{mix}$  (1.06 at 15 V).

The peak channel number dependence is shown in Fig. 2 and is within the limits set by  $M_e$  and  $M_h$ . In fact, the dependence is in good agreement with  $M_{mix}$ , which was calculated using the experimental data of  $M_e$  and  $M_h$  as well as the X-ray absorption coefficient for  $\text{Al}_{0.8}\text{Ga}_{0.2}\text{As}$  ( $639\text{ cm}^{-1}$  at 5.9 keV) and confirms that the increase in the X-ray peak gain with reverse bias is due to avalanche multiplication.

The Full Width at Half Maximum (FWHM) for each spectra in Fig. 3 was deduced by fitting a Gaussian of the main peak using IDL [8], as shown in Fig. 4 (the inset plots FWHM versus reverse bias). An energy resolution of  $\sim 1.5$  keV FWHM (reverse bias of 20 V) is not sufficient to resolve the Mn  $K_\alpha$  and  $K_\beta$  peaks (5.9 and 6.4 keV, respectively) emitted by the  $^{55}\text{Fe}$  source and is modest compared to 130 eV of a CCD cooled to  $-90^\circ\text{C}$  [9]. Yet diodes with such modest spectral resolution could be

extremely useful in a number of applications where room temperature operation is required.

As the multiplication factor increases with bias voltage, there appears to be a growing peak at higher energy, causing the X-ray spectrum to deviate from an ideal Gaussian curve. Fig. 4 compares the spectra from the  $^{55}\text{Fe}$  source for a bias voltage 20V, where the shape is approximately Gaussian and the distortion caused by the multiplication is small (the low energy side is affected by the detector noise) whereas the spectra for a bias voltage of 26 V has significantly deviated from the Gaussian shape. For reference the solid line is a true Gaussian with a FWHM of 1.45 eV. Also shown in the inset of Figure 4 is the dependence of the FWHM of the main X-ray peak which shows a general trend of decreasing FWHM with increasing reverse bias (*increasing gain*); a beneficial effect of the reduced influence of the detector noise over the X-ray peak as reverse bias increases.

The benefits of higher bias voltages in separating the X-ray peak from the noise peak and reducing FWHM values are clear in Figs. 3 and 4, respectively. However these improved characteristics are tempered by the appearance of a secondary peak at higher energy, which results in the X-ray spectrum being skewed from an ideal Gaussian shape. The non-Gaussian shape at high bias voltages degrades the energy resolution, which would limit the diode's use in spectroscopic applications. The secondary peak arises from distinct peaks in distribution of multiplication factor, when carrier dead space effects are significant in the avalanche process, as in the case of our  $\text{Al}_{0.8}\text{Ga}_{0.2}\text{As}$  diode with a relatively narrow avalanche region. However, the secondary peak is expected to be less pronounced in X-ray spectra of future more-optimised diodes with a much wider avalanche region for enhanced detection efficiency since carrier dead space effects become less significant with increasing width of the avalanche region [10].

#### **4. Diode design and X-ray detection efficiency**

Although the diodes used in this work were not specifically designed for X-ray absorption, it is informative to investigate how the diode design affects the X-ray detection efficiency,  $Q_d$ . The efficiency of the diodes is, in part, determined by the transmission and absorption in the various material layers (Table 1). If we assume, for simplicity, that only the top three layers play significant parts in the diode's efficiency for incident X-rays and that the charge collection efficiency from the  $i$  layer

is 100%, we can then calculate the transmission through the top two layers and the absorption in the third layer to estimate the efficiency using

$$Q_d = e^{-\mu_1 t_1} e^{-\mu_2 t_2} (1 - e^{-\mu_3 t_3}), \quad (1)$$

where  $\mu_i$  and  $t_i$  are the absorption coefficient and thickness for the  $i^{\text{th}}$  layer. The calculated efficiency used the absorption coefficients (as a function of energy) of materials GaAs and  $\text{Al}_{0.8}\text{Ga}_{0.2}\text{As}$  and the effects of the various absorption edges for each of the elements Al, Ga, and As. The energies for absorption edges of Ga-K, Ga-L<sub>I</sub>, Ga-L<sub>II</sub>, Ga-L<sub>III</sub>, As-K, As-L<sub>I</sub>, As-L<sub>II</sub>, As-L<sub>III</sub>, and Al-K are 10.367, 1.299, 1.143, 1.116, 11.867, 1.527, 1.359, 1.323, and 1.558 keV, respectively. A density of  $\sim 4.07 \text{ gcm}^{-3}$  was assumed for  $\text{Al}_{0.8}\text{Ga}_{0.2}\text{As}$  [11,12]. Note that Eqn. (1) may underestimate the efficiency because it ignores collection of carriers generated in layers 1, 2 and 4. Although these carriers are generated outside the depletion region, some of them can still diffuse to the depletion edges and hence contribute to the signal.

A number of designs, which are summarised in Table 2, were evaluated using Eqn. (1). Their detection efficiency versus energy characteristics are compared in Fig. 5. Parameters used for design A match the  $\text{Al}_{0.8}\text{Ga}_{0.2}\text{As}$  diode used in this work. Results of designs B and C illustrates the improvement, especially in the high energy range, that can be achieved by increasing the thickness of the  $i$  layer to  $5\mu\text{m}$  or  $20\mu\text{m}$ . Overall detection efficiency is improved if the diode is designed to have (a) minimised absorption in the top two layers (thin Layers 1 and 2), and (b) maximised absorption in the  $i$  layer (thick Layer 3).

One would also expect the higher density of  $\text{Al}_{0.8}\text{Ga}_{0.2}\text{As}$  to offer better efficiency for higher energy X-rays than a comparable silicon detector. Calculated detection efficiency versus energy characteristics for a simple Si layer of  $20 \mu\text{m}$  thickness is also shown in Fig. 5. Although the Ga and As L edges (1.1 - 1.3 keV) reduce the detection efficiency below 1 keV for  $\text{Al}_{0.8}\text{Ga}_{0.2}\text{As}$  diode when compared to the silicon diode, there is improved detection for X-rays above 3 keV. We also note that the Si detection efficiency curve has a prominent Si-K edge, which would be undesirable in some X-ray analysis applications.

## 5. Conclusions

We present experimental X-ray spectra of a  $^{55}\text{Fe}$  radioactive source measured by  $\text{Al}_{0.8}\text{Ga}_{0.2}\text{As}$  diodes operated at room temperature and at different reverse biases. Increased signal-to-noise ratio, an intended desirable effect of

avalanche multiplication, was observed in the X-ray measurements and analysed using experimental avalanche multiplication data. A modest energy resolution (FWHM of 1.47 keV at 5.9 keV with a bias voltage of 20V) was obtained at room temperature.  $\text{Al}_{0.8}\text{Ga}_{0.2}\text{As}$  diodes with a thicker depletion region ( $>10\mu\text{m}$ ) and having an optimised avalanche multiplication design are promising detectors for photon counting in soft X-ray spectroscopy.

## References

- [1] A. K. Saxena, Phys. Status Solidi B 105 (1981) 777.
- [2] B. K. Ng et al, IEEE Trans. Electron Devices 48 (2001) 2198.
- [3] G. E. Stillman and C. M. Wolfe, in: R. K. Willardson and A. C. Beer (Eds.), Semiconductors and Semimetals, vol. 12, Academic Press, New York, 1977, pp. 291-393.
- [4] J. Kataoka et al, Nucl. Inst. Meth. A 541 (2005) 398-404
- [5] Wafer Technology Ltd, 34 Maryland Road, Tongwell, Milton Keynes, Bucks, MK15 8HJ, United Kingdom
- [6] S. Adachi, J. Appl. Phys. 58 (1985) R1-R29.
- [7] M. H. Woods et al., Solid State Electronics 16 (1973) 381-394.
- [8] ITT Visual Information Solutions, Venture House, 2 Arlington Square, Downshire Way, Bracknell, Berkshire RG12 1WA, United Kingdom
- [9] H. Nakajima et al., Nucl. Inst. Meth. A 541 (2005) 365
- [10] K. F. Li et al., IEEE Trans. Electron Devices 45 (1998) 2102-2107
- [11] G. F. Knoll, Radiation detection and measurement, 3<sup>rd</sup> Ed. John Wiley and Sons, Inc., 2000, ISBN 0-471-07338-5.
- [12] <http://physics.nist.gov/PhysRefData/contents-xray.html>

## Tables

Layer	Material	Thickness ( $\mu\text{m}$ )	Dopant	Type	Doping density ( $\text{cm}^{-3}$ )
1	GaAs	0.01	Be	P	$2 \times 10^{18}$
2	$\text{Al}_{0.8}\text{Ga}_{0.2}\text{As}$	0.92	Be	P	$4 \times 10^{17}$
3	$\text{Al}_{0.8}\text{Ga}_{0.2}\text{As}$	0.58	Undoped	P	$5 \times 10^{16}$
4	$\text{Al}_{0.8}\text{Ga}_{0.2}\text{As}$	1.0	Si	N	$2 \times 10^{18}$
5	GaAs	0.25	Si	N	$2 \times 10^{18}$
GaAs $n^+$ substrate					

Table 1: Wafer details of the  $\text{Al}_{0.8}\text{Ga}_{0.2}\text{As}$  ppn diode used in this work.

Design	Layer	Material	Thickness ( $\mu\text{m}$ )
A	1	GaAs	0.01
	2	AlGaAs	0.92
	3	AlGaAs	0.58
B	1	GaAs	0.01
	2	AlGaAs	0.01
	3	AlGaAs	5
C	1	GaAs	0.01
	2	AlGaAs	0.01
	3	AlGaAs	20

Table 2: Parameters used in various designs to evaluate detector efficiency. Parameters for design A matches the  $\text{Al}_{0.8}\text{Ga}_{0.2}\text{As}$  diode studied in this work.

### Figure captions

Fig. 1: Optical photograph of the fabricated circular mesa devices.

Fig. 2:  $M_e$  and  $M_h$  (left axis) versus reverse bias of the devices obtained from photomultiplication measurements. Scaled peak X-ray channel number (right axis) versus reverse bias characteristics is in agreement with the calculated  $M_{mix}$ .

Fig. 3: Room temperature spectra from a  $^{55}\text{Fe}$  source for D2 as a function of reverse bias voltage.

Fig. 4: X-ray spectra from a  $^{55}\text{Fe}$  radioactive source taken with device D2 at room temperature after avalanche multiplication was taken into account. Squares: bias voltage 20V, diamond: bias voltage 26V. The solid line is a true Gaussian with a FWHM of 1.45. The inset plots FWHM versus reverse bias.

Fig 5. Comparison of calculated absorption efficiency of three  $\text{Al}_{0.8}\text{Ga}_{0.2}\text{As}$  detectors (Designs A, B, and C, see Table 2) and a 20 $\mu\text{m}$  thick Si layer.

## Figures J.E. Lees et al. AlGaAs diodes for X-ray spectroscopy

Figure 1

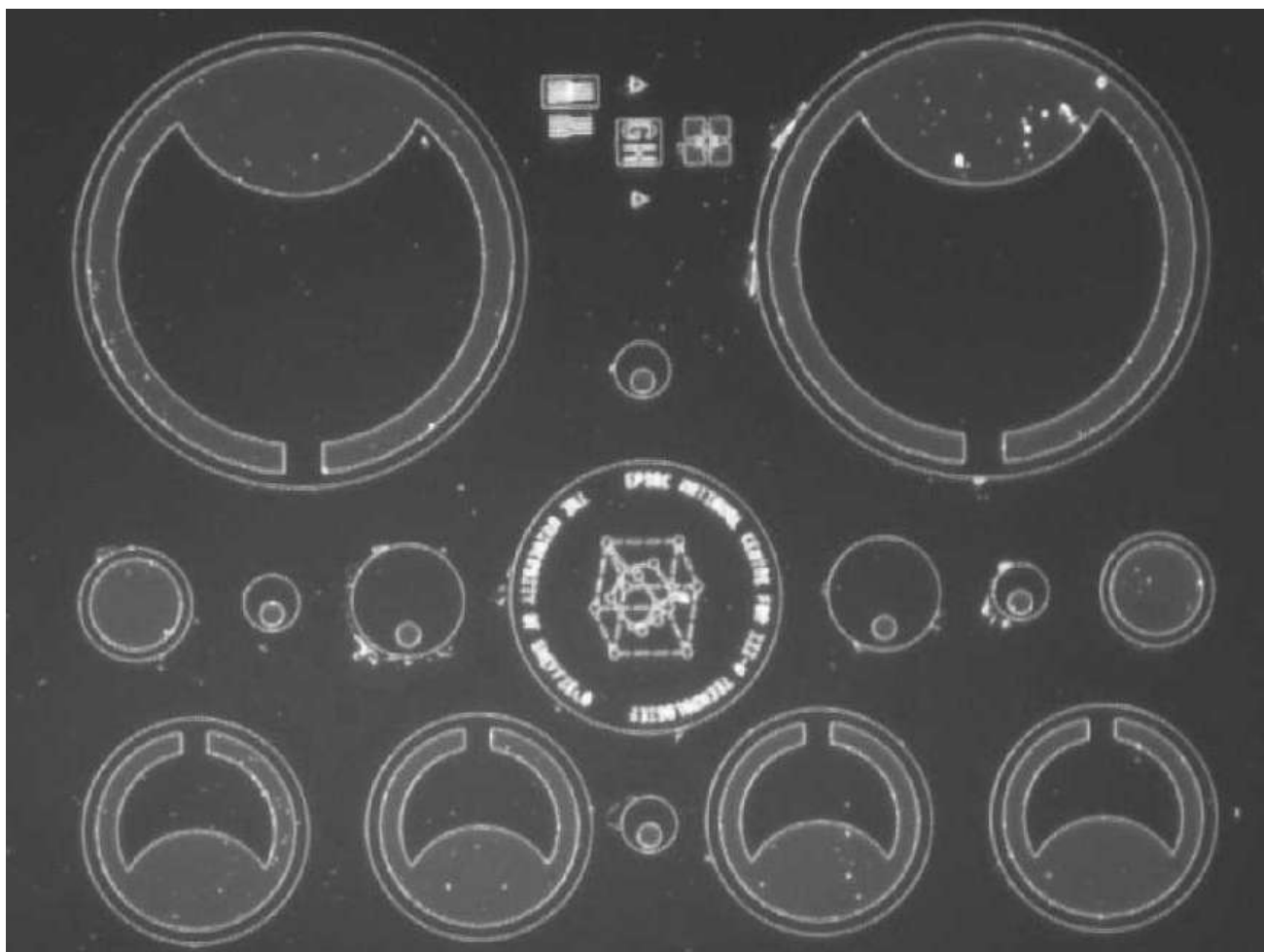
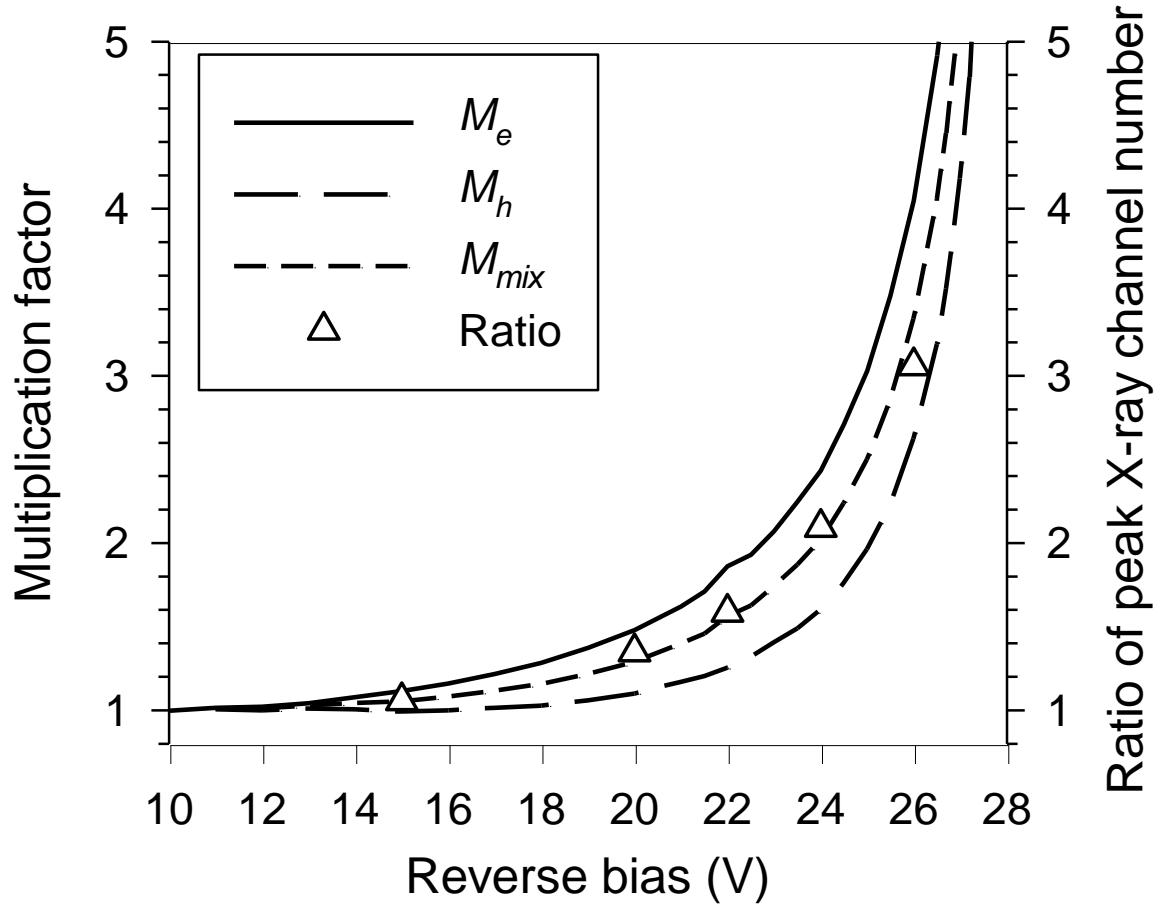


Figure 2



**Figure 3**

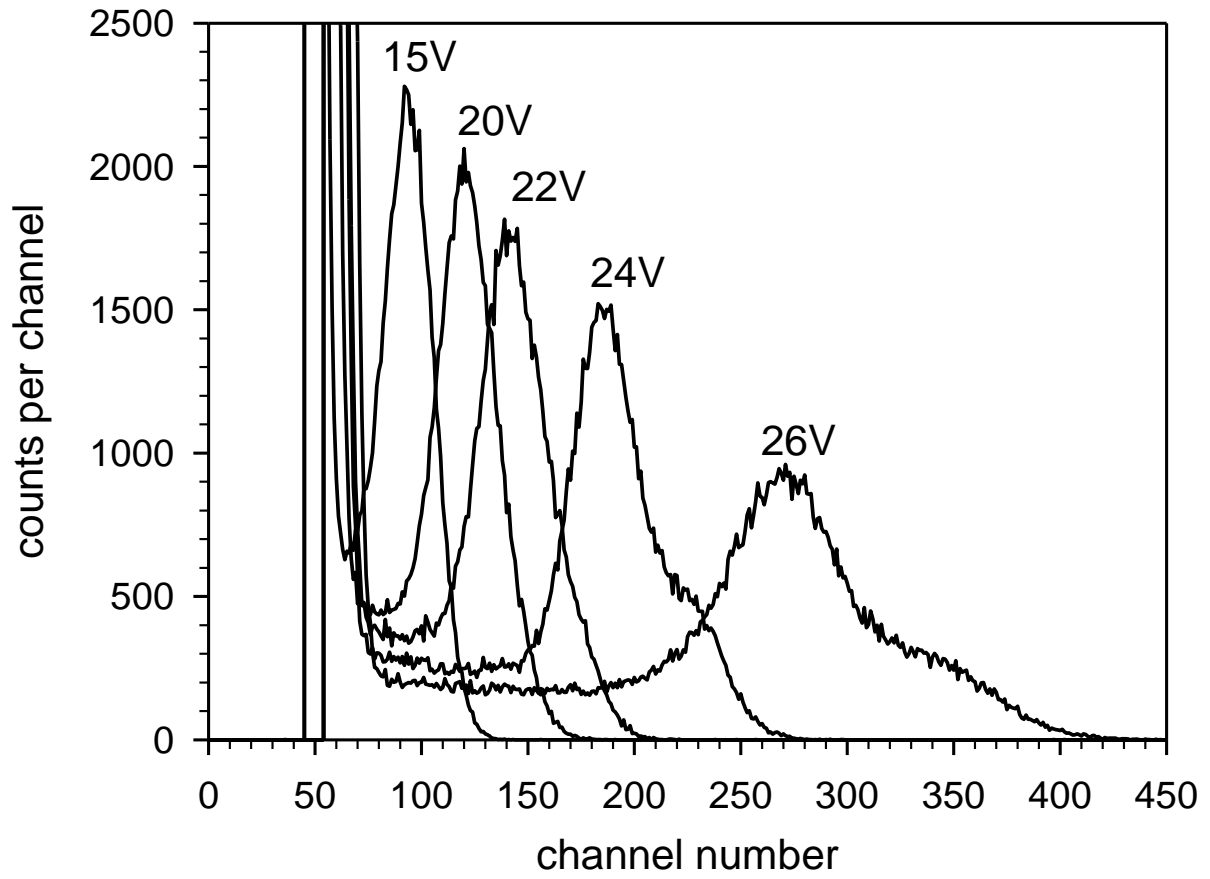


Figure 4.

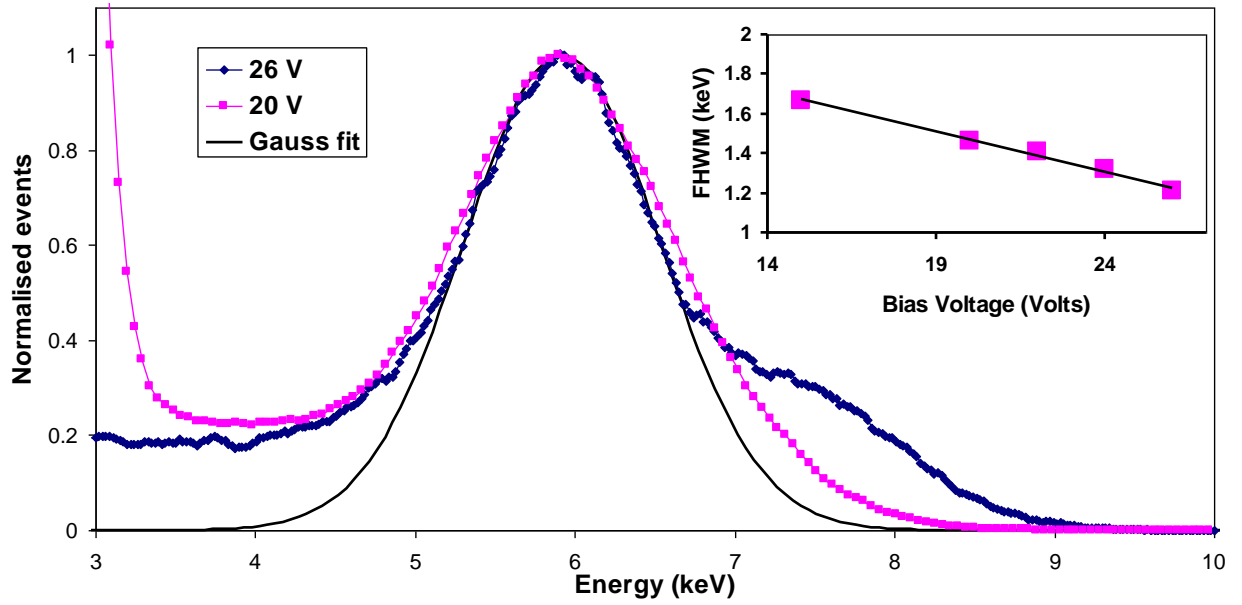


Figure 5

